Journal of Statistical Physics, Vol. 56, Nos. 5/6, 1989

Transfer Matrix Spectrum for the Finite-Width Ising Model with Adjustable Boundary Conditions: Exact Solution

D. B. Abraham,[1,2] L. F. Ko,[1] and N. M. Švrakić[1]

Received March 13, 1989; final April 24, 1984

Using the spinor approach, we calculate exactly the complete spectrum of the transfer matrix for the finite-width, planar Ising model with adjustable boundary conditions. Specifically, in order to control the boundary conditions, we consider an Ising model wrapped around the cylinder, and introduce along the axis a "seam" of defect bonds of variable strength. Depending on the boundary conditions used, the mass gap is found to vanish algebraically or exponentially with the size of the system. These results are compared with recent numerical simulations, and with random-walk and capillary-wave arguments.

KEY WORDS: Ising model; finite-size transfer matrix; spectral properties; mass gap; adjustable boundary conditions.

1. INTRODUCTION

During the past several years the theory of finite-size effects, and of finite-size scaling in general,[1–3] has emerged as a particularly useful tool in the studies of critical and noncritical properties of a variety of two- and three-dimensional (3D) lattice models. An important application of the theory is in Monte Carlo simulations,[4] where, in order to estimate thermodynamic limit (infinite-size) quantities, one needs a proper extrapolation procedure which preferably has theoretical justification. A typical example of this is the surface tension, for which a finite-size scaling function is needed. On the basis of their Monte Carlo simulations, Mon and Jasnow[4]

[1] Department of Physics, Clarkson University, Potsdam, New York 13676.
[2] Permanent address: Department of Theoretical Chemistry, Oxford University, Oxford, OX1 3UB, United Kingdom.

0022-4715/89/0900-0563$06.00/0 © 1989 Plenum Publishing Corporation

guessed the form, which was subsequently shown[5] to be a rather accurate estimate by an exact calculation of this function.

Another application is in numerical transfer matrix (TM) methods[6] applied to strips of finite width but infinite length. The extrapolation is then made over the strip width; scaling arguments have to be invoked to justify this procedure. Within the transfer matrix method, the mathematical description of critical behavior is formulated in terms of the spectral properties of the TM, specifically, the asymptotic degeneracy of the largest eigenvalues. Away from criticality, the TM spectrum may yield information not only on the bulk thermodynamic quantities, but also on various interfacial properties[7–9] (below T_c). However, it has been realized that boundary condition effects play an important role in such applications and must be carefully accounted for.[10]

The effect of boundary conditions on the TM spectrum has been recently analyzed by Cabrera and Jullien,[10] who performed an extensive numerical study of the asymptotic behavior of the mass gap in the 1D quantum Ising chain with variable boundary conditions and $T < T_c$. Their study suggests that the mass gap may vanish exponentially or algebraically with increasing size of the system, and that the precise behavior depends on the boundary conditions used. Several phenomenological,[11] random walk,[12] and capillary-wave arguments[9,13] have been developed in order to explain this surprising result. Exact results for the 1D quantum Ising model in the transverse field have been available[14–16] only for free, periodic, and antiperiodic boundary conditions, so that numerical results for more general boundary conditions cannot be checked. Furthermore, by appealing to universality, one can expect the equivalence between the finite-size properties of 1D quantum models and the planar Ising model; essentially, the relationship is that the 1D Ising model with perpendicular magnetic field is obtained in the limit of extreme anisotropy of the planar Ising model.[2] Such a limit undoubtedly suppresses certain scattering events in the fermion picture and therefore should not be viewed uncritically. Nevertheless, one has some reason to believe that the numerical results of Cabrera and Jullien[10] indeed apply to the isotropic Ising model with appropriate boundary conditions.

In this work we study the finite-size planar Ising model and consider a finite-dimensional TM between rows, each having M spins, with adjustable boundary conditions. By this we mean that the coupling between the Mth and the first spin in any row, denoted gJ_2, is different from the value between any other pair, which is denoted by J_2. Thus, we generalize earlier work by one of the authors[17] in which the considerably simpler problem, with $g = 0$, was analyzed. Another result,[18] related to this last one by duality, as it later transpired, is the spectrum of the transfer

matrix with the spins at the end of the row fixed. Here we consider a finite-size, $M \times \infty$, square lattice 2D Ising strip with adjustable boundary conditions (see below) and calculate *exactly* the complete set of eigenvalues of the corresponding TM. The TM eigenvalues will be denoted Λ_j, with

$$\Lambda_0 > \Lambda_1 > \Lambda_2 \cdots \tag{1.1}$$

where some of the eigenvalues may be multiply degenerate, but the maximal one is simple by the Perron–Frobenius theorem. Finite-size correlation lengths corresponding to spectral gaps are introduced by[7]

$$\xi_j(M) = [\ln(\Lambda_0/\Lambda_j)]^{-1} \tag{1.2}$$

with $j = 1, 2, \ldots$. The phase transition is typically accompanied by the divergence, as $M \to \infty$, of one or more correlation lengths $\xi_j(M)$. For example, in the periodic Ising cylinders, the first-order phase transition is associated with exponential divergence of $\xi_1(M)$ only.[8] The other extreme is the critical point spectrum characterized by the linear divergence[1] of an unbounded number of $\xi_j(M)$.

In addition to the finite-size correlation length $\xi_1(M)$, it is customary to consider the behavior of the mass gap $m(M)$, defined by

$$m(M) \sim 1/\xi_1(M) \tag{1.3}$$

which vanishes in the limit $M \to \infty$. From the work of Onsager[19] and Kaufman,[20] it is known that the mass gap of the Ising strip with *periodic* boundary conditions vanishes exponentially as

$$m(M) \simeq CM^{-\alpha} \exp(-\sigma M) \tag{1.4}$$

with $\alpha = 1/2$, while $\sigma = \tau$ is the surface tension of an interface orthogonal to the cylinder axis. This suggests a phenomenological picture[5,9,13] of a "gas" of interfaces orthogonal to the axis and separated by the average distance $[m(M)]^{-1} \sim \xi_1(M)$. That is, for $T < T_c$, the cylinder breaks into domains of size $\xi_1(M)$, with + and − magnetizations. In this work we show that for general boundary conditions, the mass gap indeed vanishes according to (4), but with variable values of α and σ. Furthermore, for certain boundary conditions, $\sigma = 0$, and the decay of the mass gap becomes algebraic. More generally, $0 \leqslant \sigma \leqslant \tau$. The comparison of our results with numerical[10] and phenomenological[9,11-13] arguments will be made as we proceed. Some of the results described in this work have been previously published in a shorter form.[21]

The presentation is organized as follows. In Section 2 we define the finite-size Ising model with adjustable boundary conditions and summarize

our results for the mass gap. In the same section we express the TM in the form of the rotation matrix in spinor space. In Section 3 we briefly describe the spinor approach. The rotation matrix is diagonalized in Section 4 and the quantization condition for the allowed wavenumbers is derived. Section 4 presents the results for the spectrum of the rotation matrix. The spectrum of the TM is given in Section 6. In Section 7 the results for the mass gap are obtained from the ratio of the two largest eigenvalues of the TM. Finally, in Section 8, we present qualitative arguments which emphasize the physical picture behind the finite-size behavior of the mass gap.

2. DEFINITION OF THE MODEL AND SUMMARY OF THE RESULTS

Consider a 2D Ising square lattice wrapped on a cylinder of circumference M, as shown in Fig. 1. The spins interact via nearest-neighbor ferromagnetic interactions J_1 and J_2 parallel and orthogonal to the cylinder axis, respectively. In addition, a set of modified bonds $\tilde{J}$ different from J_2 is introduced in a row parallel to the axis, as shown by thick lines in Fig. 1. It is customary to denote $g = \tilde{J}/J_2$. By changing the value of the parameter g, one can control the boundary conditions. For instance, the values $g = -1, 0, +1$ correspond to antiperiodic, free, and periodic boundary conditions, respectively. In this work we will allow this parameter to assume arbitrary real values $-\infty < g < +\infty$.

Our results for the mass gap can be summarized as follows. For all values of g, the gap vanishes according to (1.4), with α and σ varying with g. In particular, we establish by exact calculation:

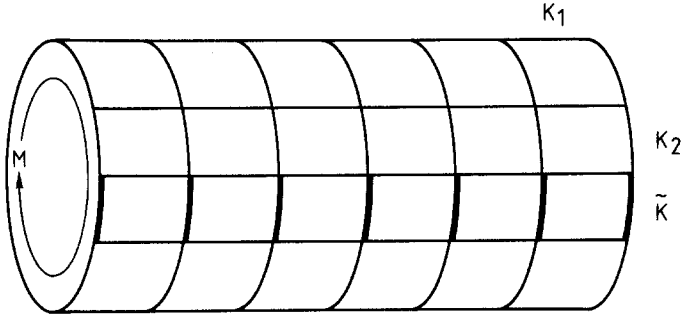

Fig. 1. The boundary of a two-dimensional Ising model with nearest-neighbor reduced couplings K_1 and K_2 as modified by an adjustable coupling $\tilde{K}$ along the axis of the cylinder with circumference M.

1. For all $g>0$, the gap vanishes exponentially, with $\alpha=1/2$ and $\sigma=\tau$.
2. For $-1<g\leqslant 0$, the decay is still exponential, with $\alpha=0$, while $0<\sigma\leqslant\tau$ depends on g and the temperature. The explicit expression is given by (6.12) below, and the graph of σ is shown in Fig. 6.
3. For $g=-1$, the mass gap vanishes algebraically, with $\sigma=0$ and $\alpha=2$.
4. For all $g<-1$, the algebraic decay ($\sigma=0$) persists, with $\alpha=3$.

Let us now turn to the derivation of these and other results. In order to analyze the model described, we consider the transfer matrix in the direction parallel to the cylinder axis. Our approach is based on the spinor technique[20] of Kaufman and Onsager. (A more transparent fermion technique seems to be unsuitable for this problem.)

In terms of the Pauli matrices σ_m^α ($\alpha=x, y, z$), the matrix associated with the horizontal bonds, i.e., bonds between columns, is expressed in its usual form

$$V_1=\exp\left(-K_1^*\sum_1^M\sigma_m^z\right) \tag{2.1}$$

with $K_1=J_1/k_BT$, and the dual coupling defined by $\sinh 2K_i \sinh 2K_i^*=1$, for $i=1, 2$. In the vertical direction we consider a ring of couplings $K_2=J_2/k_BT$, with one altered bond $\tilde{K}=\tilde{J}/k_BT$. The corresponding matrix is

$$V_2=\exp\left(K_2\sum_{m=1}^{M-1}\sigma_m^x\sigma_{m+1}^x+\tilde{K}\sigma_M^x\sigma_1^x\right) \tag{2.2}$$

Note that the presence of $\tilde{K}$ breaks the translational symmetry of the problem, except in the special cases corresponding to periodic and antiperiodic boundary conditions.

Consider now the full symmetrized TM given by $V=V_1^{1/2}V_2V_1^{1/2}$. In the spinor approach of Kaufman and Onsager,[20] the TM is expressed in terms of operators (spinors) Γ, defined by

$$\Gamma_{2j-1}=\prod_{i=1}^{j-1}(-\sigma_i^z)\,\sigma_j^x, \qquad \Gamma_{2j}=\prod_{i=1}^{j-1}(-\sigma_i^z)\,\sigma_j^y \tag{2.3}$$

where the spinors satisfy the anticommutation relation $[\Gamma_i, \Gamma_j]_+=2\delta_{ij}$. Using (2.1)–(2.3), one can write the matrices V_1 and V_2 in the form

$$V_1=\prod_{j=1}^{M}\exp(iK_1^*\Gamma_{2j-1}\Gamma_{2j}) \tag{2.4}$$

and

$$V_2 = \prod_{j=1}^{M-1} \exp(iK_2 \Gamma_{2j} \Gamma_{2j+1}) \exp(-i\tilde{K} \Gamma_{2M} \Gamma_1 P_M) \tag{2.5}$$

where the parity operator $P_M = \Gamma_1 \Gamma_2 \cdots \Gamma_{2M}$ commutes (anticommutes) with any product of an even (odd) number of Γ's.

From the definition (2.3), and with the use of the commutation properties of Γ's, the following relations are easily derived:

$$e^{iK\Gamma_m\Gamma_n} \Gamma_j e^{-iK\Gamma_m\Gamma_n} = \begin{cases} \Gamma_j, & \text{for } j \neq m, n \\ \Gamma_m \cosh 2K - \Gamma_n (i \sinh 2K), & \text{for } j = m \\ \Gamma_m (i \sinh 2K) + \Gamma_n \cosh 2K, & \text{for } j = n \end{cases} \tag{2.6}$$

indicating that V_1 can be expressed as a rotation. Specifically, in the spinor space spanned by the vectors $(\Gamma_1, \ldots, \Gamma_{2M})$, the matrix V_1 can be represented by a $2M$-dimensional rotation matrix R_1,

$$V_1^{-1} \Gamma_j V_1 = \sum_k (R_1)_{kj} \Gamma_j \tag{2.7}$$

From (2.6) it is evident that R_1 has a 2×2 block-diagonal form

$$R_1 = \begin{pmatrix} u_1 & 0 & \cdots & 0 \\ 0 & u_1 & \cdots & 0 \\ \vdots & \vdots & \ddots & \vdots \\ 0 & 0 & \cdots & u_1 \end{pmatrix} \tag{2.8}$$

with

$$u_1 = \begin{pmatrix} \cosh 2K_1^* & i \sinh 2K_1^* \\ -i \sinh 2K_1^* & \cosh 2K_1^* \end{pmatrix} \tag{2.9}$$

acting on the $(\Gamma_{2j-1}, \Gamma_{2j})$ space for $j = 1, \ldots, M$. Similarly, V_2 can be expressed as a combination of two rotation operators acting in the even and odd parity subspaces,

$$V_2 = \tfrac{1}{2}(1 + P_M) V_{2+} + \tfrac{1}{2}(1 - P_M) V_{2-} \tag{2.10}$$

In the special case $\tilde{K} = K_2$ (periodic boundary conditions), V_{2+} and V_{2-} become anticyclic and cyclic, respectively. The rotation matrices for $V_{2\pm}$, denoted $R_{2\pm}$, are also block diagonal, but with

$$u_2 = \begin{pmatrix} \cosh 2K_2 & i \sinh 2K_2 \\ -i \sinh 2K_2 & \cosh 2K_2 \end{pmatrix} \tag{2.11}$$

and have the form

$$R_{2\pm} = \begin{pmatrix} \cosh 2\tilde{K} & 0 & \cdots & \mp i \sinh 2\tilde{K} \\ 0 & u_2 & \cdots & 0 \\ \vdots & \vdots & \ddots & \vdots \\ \pm i \sinh 2\tilde{K} & 0 & \cdots & \cosh 2\tilde{K} \end{pmatrix} \tag{2.12}$$

The full transfer matrix V can thus be decomposed into its even and odd components, with $V_- = V_1^{1/2} V_{2-} V_1^{1/2}$ and $V_+ = V_1^{1/2} V_{2+} V_1^{1/2}$ with rotational representation in the Γ_j space as in (2.7),

$$V_\pm \Gamma V_\pm^{-1} = R\Gamma \tag{2.13}$$

Since the rotation matrices for $V_{2\pm}$ are related by a change of signs of $\tilde{K}$, we consider only the odd subspace V_- and diagonalize $R_- = R_1^{1/2} R_{2-} R_1^{1/2}$ for arbitrary $\tilde{K}$. The corresponding results for the even subspace V_+ are easily obtained by inverting the sign of $\tilde{K}$. The diagonalization of the rotation matrix is described in Section 4; the connection between the eigenvalues of the TM and the eigenvalues of $R_\pm$ is discussed in Section 6.

3. SPINOR APPROACH

Kaufman gave an analysis of the eigenvalue problem for symmetrized form of $V_1 V_2$ which is based on the theory of spinor representation[20] of the orthogonal group and may be thought of as a rigorous and compact version of the equation-of-motion method. It is of great elegance and is completely general in the present context. There are special features of the present problem, however, which make greater simplicity possible; what is needed is a little linear algebra. In the spirit of Occam's razor, we will follow this latter course in the present article.

In the previous section we showed that the transfer operator V induces a rotation R in the linear vector space spanned by the spinors. We start with a proposition about the canonical form of R.

Proposition 1. R can be reduced to the canonical block-diagonal form

$$R = \begin{pmatrix} H_1 & 0 & \cdots & 0 \\ 0 & H_2 & \cdots & 0 \\ \vdots & \vdots & \ddots & \vdots \\ 0 & 0 & \cdots & H_M \end{pmatrix} \tag{3.1}$$

where

$$H_j = \begin{pmatrix} \cosh \gamma_j & i \sinh \gamma_j \\ -i \sinh \gamma_j & \cosh \gamma_j \end{pmatrix} \tag{3.2}$$

with γ real, by a real, orthogonal transformation S:

$$R = SHS^T \tag{3.3}$$

Proof. First, we examine the eigenvalue problem for R:

$$Ry = \lambda y \tag{3.4}$$

We notice that $R = R^\dagger$, and $\det R = 1$. This means that the eigenvalues are real and occur in pairs $\exp(\pm\gamma)$. With orthogonality of R, we get

$$Ry^* = \lambda^{-1} y^* \tag{3.5}$$

We can always normalize the y_j corresponding to the indexed eigenvalue λ_j to get

$$y_i^\dagger y_j = \delta_{ij} \tag{3.6}$$

and we get from (3.5) that

$$y_i^T y_j = 0 \tag{3.7}$$

for all i, j. With the notation

$$Ry_j = e^{\gamma_j} y_j \tag{3.8}$$

to supplement (3.4), we get with (3.5) that

$$R(y_j + y_j^*) = \cosh \gamma_j (y_j + y_j^*) + \sinh \gamma_j (y_j - y_j^*) \tag{3.9}$$

and

$$R(y_j - y_j^*) = \cosh \gamma_j (y_j - y_j^*) - \sinh \gamma_j (y_j + y_j^*) \tag{3.10}$$

Let us define

$$\phi_j = (y_j + y_j^*)/\sqrt{2}, \qquad \psi_j = -i(y_j - y_j^*)/\sqrt{2} \tag{3.11}$$

We see from (3.6) and (3.7) that

$$\phi_j^T \phi_j = \psi_j^T \psi_j = \delta_{ij}; \qquad \psi_j^T \phi_j = 0 \tag{3.12}$$

Taking (3.9)–(3.12), we get (3.1) with the real orthogonal transformation given by

$$S = (\psi_1 \phi_1; \psi_2 \phi_2; \ldots; \psi_M \phi_M) \tag{3.13}$$

where each ψ_j, ϕ_j is a column vector with $2M$ components, given in terms of the eigenvalue problem for R by (3.11), completing the proof.

Proposition 2. Define

$$\hat{\Gamma} = S^T \Gamma \tag{3.14}$$

Then the $\hat{\Gamma}$ are spinors and

$$V \hat{\Gamma}^T V^{-1} = \hat{\Gamma}^T H \tag{3.15}$$

where H is given by (3.1).

Proof. Orthogonality of S gives

$$[\hat{\Gamma}_i, \hat{\Gamma}_j]_+ = 2\delta_{ij} \tag{3.16}$$

The self-adjointness of each $\hat{\Gamma}_j$ follows because S is real. Thus the $\hat{\Gamma}$ are spinors.

Proposition 3. V can be written as

$$V = c \exp\left(i \sum_1^M \gamma_j \hat{\Gamma}_{2j-1} \hat{\Gamma}_{2j} \right) \tag{3.17}$$

where c is an arbitrary real number (see below).

Proof. Use Proposition 2 with (2.5), (2.9), and (2.10).

Remark. Let us define operators X_j by

$$\hat{\Gamma}_{2j-1} = X_j^\dagger + X_j, \qquad \hat{\Gamma}_{2j} = -i(X_j^\dagger - X_j) \tag{3.18}$$

Then, the X_j are Fermi operators and V takes the form

$$V = c \exp\left[-\frac{1}{2} \sum_1^M \gamma_j (2X_j^\dagger X_j - 1) \right] \tag{3.19}$$

Evidently, the product of eigenvalues is

$$c^{2M} = \det V_1 \det V_2 \tag{3.20}$$

from which we get $c = 1$, since the maximum eigenvalue is positive.

4. DIAGONALIZATION OF THE ROTATION MATRIX

Our next step is to find the eigenvalues of the symmetrized rotation matrix $R = R_- = R_1^{1/2} R_2 R_1^{1/2}$. The procedure is similar to that of ref. 17, in which the spectrum for the free boundary case is obtained.

We have seen that the matrix R has the following properties: Because R is Hermitean, its eigenvalues are real; because $RR^* = I$, the inverse of an eigenvalue is also an eigenvalue, with eigenvectors given by complex conjugation. Consequently, the $2M$ eigenvalues of R can be written in the form $\exp(\pm\gamma_j)$, with γ_j real.

In order to obtain the eigenvalues and eigenvectors of R, it proves convenient to consider first the solution of the eigenproblem

$$L\mathbf{x} = (R_2 - e^{\gamma} R_1^{-1})\mathbf{x} = 0 \tag{4.1}$$

where $\mathbf{x}$, the eigenvector of L, is related to $\mathbf{y}$, the eigenvector of R, by $\mathbf{y} = R_1^{-1/2}\mathbf{x}$.

To simplify the notation, define

$$\begin{aligned} a &= e^{\gamma} \cosh 2K_1^*, & b &= -ie^{\gamma} \sinh 2K_1^* \\ c &= \cosh 2K_2, & d &= -i \sinh 2K_2 \\ \tilde{c} &= \cosh 2\tilde{K}, & \tilde{d} &= -i \sinh 2\tilde{K} \end{aligned} \tag{4.2}$$

Using the explicit expressions (2.8), (2.9), (2.11), and (2.12), for R_1 and R_2, we obtain from the eigenvalue problem (4.1) that the components of $\mathbf{x}$ satisfy the system of second-order recurrences

$$-bx_{2j-1} + (a-c)\, x_{2j} + dx_{2j+1} = 0 \tag{4.3a}$$

$$-dx_{2j} + (a-c)\, x_{2j+1} + bx_{2j+2} = 0 \tag{4.3b}$$

for $j = 1, \ldots, M-1$. The solutions of these equations are subject to boundary conditions

$$(a-\tilde{c})\, x_1 + bx_2 - \tilde{d}x_{2M} = 0 \tag{4.4a}$$

$$-bx_{2M-1} + (a-\tilde{c})\, x_{2M} + \tilde{d}x_1 = 0 \tag{4.4b}$$

where we have used the notation (4.2). The recurrence relations (4.3) are identical to those for the free-boundary case considered in ref. 17. However, the boundary conditions (4.4) are different, as expected. Note also that the symmetry

$$x_{2j+1} = i\beta x_{2M-2j} \tag{4.5a}$$

$$x_{2j} = -i\beta x_{2M+1-2j} \tag{4.5b}$$

with $\beta^2 = 1$ persists for general values of $\tilde{K}$. We seek the solutions of (4.3) in the general form

$$x_{2j} = A_1 z^{2j} + A_2 z^{-2j} \tag{4.6a}$$

$$x_{2j+1} = i\beta(A_2 z^{2(j-M)} + A_1 z^{2(M-j)} \tag{4.6b}$$

with

$$A_1/A_2 = -i\beta z^{-1-2M} F(z), \qquad F(z) = (dz - bz^{-1})/(a-c) \tag{4.6c}$$

For the system of equations (4.3) to possess the nontrivial solution, the condition

$$(a-c)^2 = (dz - bz^{-1})(bz - dz^{-1}) \tag{4.7}$$

has to be satisfied. Substituting in this condition the explicit forms for a, b, c, and d from (4.2), and denoting $z^2 = \exp(i\omega)$, we obtain that $\gamma(\omega)$, from (4.1), is precisely equal to the Onsager γ dispersion function; see below.

Due to the finiteness of the system, the allowed values of ω_j will be quantized. The quantization condition is obtained after substitution of (4.6) in the boundary condition (4.4). The resulting equation can be put in a more convenient form by using (4.3b) with $j = 0$. We obtain

$$z^{2M} = -i\beta[c - \tilde{e} - dz^{-1}F(z)]/[(c-\tilde{e})\, z^{-1}F(z) + d] \tag{4.8}$$

with $\tilde{e} = \tilde{c} - i\beta d = \exp(-2\beta\tilde{K})$. The condition (4.8) can be written in a more convenient form if we observe that the right-hand side of (4.8) is unimodular and is therefore expressible in the form $\exp(iP)$, with P a real function. Substituting $z^2 = \exp(i\omega)$ in (4.8), and using the identity for unimodular functions, namely

$$\frac{C_1 + iD_1}{C_2 + iD_2} = \frac{C_2 - iD_2}{C_1 - iD_1} = \frac{C_1 + C_2 + i(D_1 - D_2)}{C_1 + C_2 - i(D_1 - D_2)}$$

$$= \frac{1 + \cos P + i \sin P}{1 + \cos P - i \sin P} \tag{4.9}$$

we obtain for the quantization condition (4.8)

$$e^{iM\omega} = \beta e^{iP(\omega, \beta g)}, \qquad \tan\frac{P(\omega, x)}{2} = Y(x) \tan\frac{\delta^*(\omega)}{2} \tag{4.10a}$$

with

$$Y(x) = \frac{\sinh[(1-x)\, K_2]}{\sinh[(1+x)\, K_2]}, \qquad g = \frac{\tilde{K}}{K_2} \tag{4.10b}$$

The function $Y(x)$ is sketched in Fig. 2. The functions $\gamma(\omega)$ and $\delta^*(\omega)$ are the elements of the Onsager hyperbolic triangle[17,19] and are given by

$$\cosh \gamma(\omega) = \cosh 2K_1^* \cosh 2K_2 - \sinh 2K_1^* \sinh 2K_2 \cos \omega \tag{4.11a}$$

$$\sinh \gamma(\omega) \cos \delta^*(\omega) = \sinh 2K_2 \cosh 2K_1^* - \cosh 2K_2 \sinh 2K_1^* \cos \omega \tag{4.11b}$$

$$\frac{\sin \omega}{\sinh \gamma(\omega)} = \frac{\sin \delta^*(\omega)}{\sinh 2K_1^*} \tag{4.11c}$$

Therefore, the quantization condition (4.10) determines the allowed values of the wavenumbers ω_j and discretizes the spectrum of the rotation matrix.

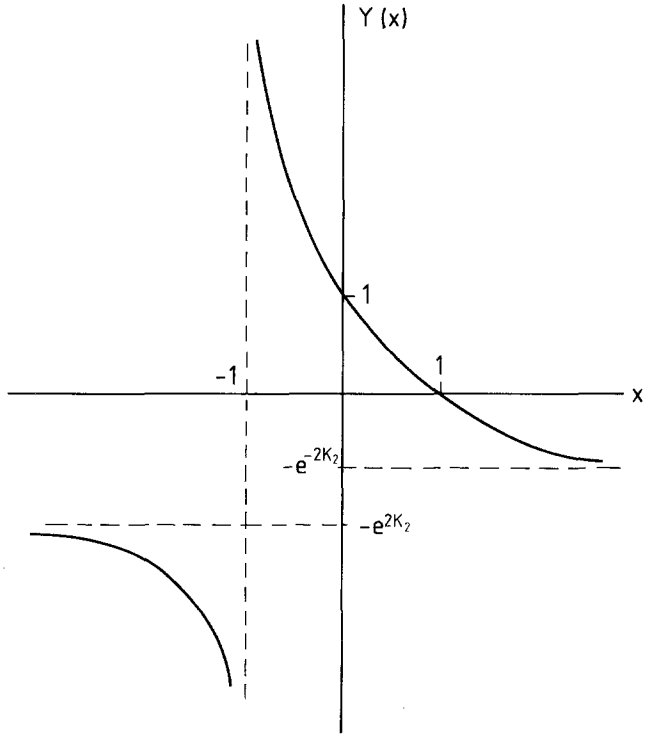

Fig. 2. Sketch of the function $Y(x)$ entering in the quantization condition (4.10).

5. SPECTRUM OF THE ROTATION MATRIX

In order to determine the spectrum of the rotation matrix we must consider the real solutions of the quantization condition (4.10). These solutions can be located graphically, as sketched in Fig. 3, by using the equivalent expression

$$\tan\frac{M\omega}{2}=\beta Y(g)\left(\tan\frac{\delta^*(\omega)}{2}\right)^{\beta} \tag{5.1}$$

Consider for simplicity the case when M is even. Clearly, there are $M/2$ solutions for $\beta=-1$. For $\beta=+1$ there are only $M/2-1$ solutions, because the values $\omega=0,\ \pi$ lead to trivial eigenvectors when substituted in the eigenvector equations (4.6). Since M solutions are expected, we seek the additional solution among the complex values of ω. This is found at $\exp(i\omega_I)=\pm\exp(-v)$, with $v>0$. Write (4.10) in the form

$$e^{-Mv}=\beta\frac{1+iY(\beta g)\tan(\delta^*/2)}{1-iY(\beta g)\tan(\delta^*/2)} \tag{5.2}$$

The left-hand side of this equation vanishes as $M\to\infty$. In this limit $\omega_I\to\omega_0$, i.e., $v\to v_0$, where the value v_0 is obtained by setting the numerator of (5.2) to zero. This gives

$$\frac{Y(\beta g)-1}{Y(\beta g)+1}=e^{i\delta^*(\omega_0)} \tag{5.3}$$

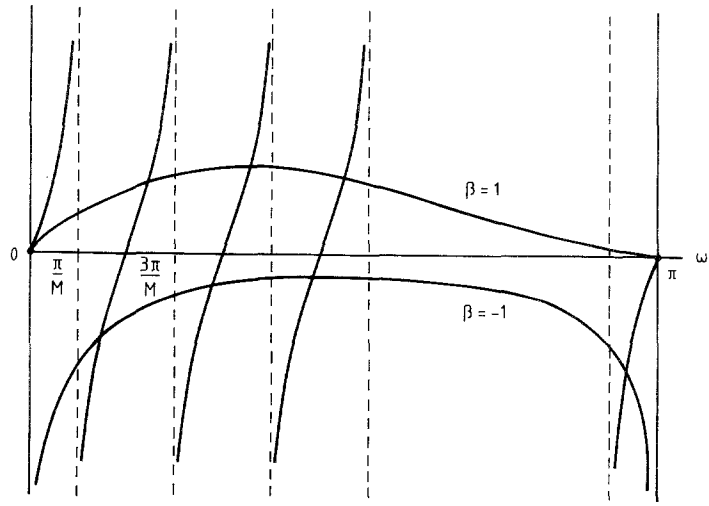

Fig. 3. A sketch of the left- and right-hand sides of Eq. (5.1). The intersections give the real wavenumbers allowed by the quantization condition (4.10).

or, equivalently,

$$-\frac{\tanh(\beta g K_2)}{\tanh K_2}=\left(\frac{B}{A}\right)^{1/2}\left[\frac{(e^{i\omega_0}-A)(e^{i\omega_0}-B^{-1})}{(e^{i\omega_0}-A^{-1})(e^{i\omega_0}-B)}\right]^{1/2} \tag{5.4a}$$

where

$$A=e^{2(K_1+K_2^*)}, \qquad B=e^{2(K_1-K_2^*)} \tag{5.4b}$$

The branch of the square root in (5.4) is chosen such that $\exp[i\delta^*(0)]=1$. For $T<T_c$, the function $\exp[i\delta^*(\omega)]$ has branch points A^{-1}, B^{-1} inside the unit circle in the $\exp(i\omega)$ plane. This function is real between -1 and 1, except in the branch cut between A^{-1} and B^{-1}, as shown in Fig. 4. Hence a solution exists for $\beta g<0$ and the complex root $i\omega_0$ is located at

$$B^{-1}<e^{i\omega_0}<1 \qquad \text{for} \quad |g|<1 \tag{5.5a}$$

and

$$-1<e^{i\omega_0}<0 \qquad \text{for} \quad |g|>1 \tag{5.5b}$$

as shown in Fig. 4. Thus, $\exp(i\omega_0)$ coincides with the branch point B^{-1} for $|g|=0$; it moves toward 1 as $|g|\to 1$, the (anti)periodic limit; it then reappears at -1 and approaches 0 as $|g|$ increases from 1^+ to $+\infty$.

More generally, let $iv_\pm$ denote the imaginary roots of (4.1) for $g\gtrless 0$ and $|g|<1$. For large but finite M, the difference $v_\pm - v_0$ is exponentially small. The first correction is obtained by iterating (5.2),

$$v_\beta - v_0 \simeq -4\beta e^{-Mv_0}[Y(|g|)-Y(|g|)^{-1}]^{-1}\left[\frac{d\delta^*}{d\omega}(iv_0)\right]^{-1} \tag{5.6}$$

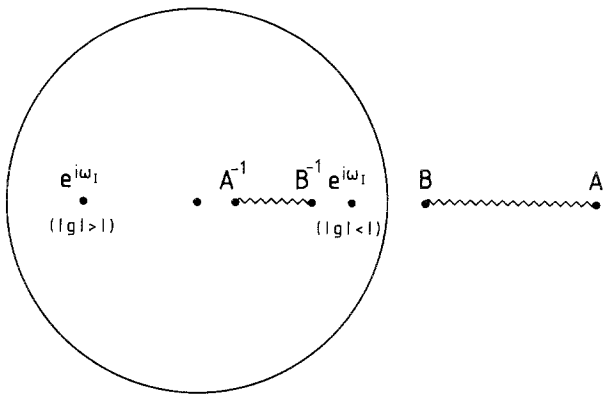

Fig. 4. The branch structure of $\exp i\delta^*(\omega)$ in the complex $\exp(i\omega)$ plane for $T<T_c$. The imaginary solutions to (4.10) are located between -1 and 0 for $|g|>1$ and between B^{-1} and 1 for $|g|<1$.

For $|g| > 1$, the right-hand side changes sign; however, the imaginary roots in this case have no influence on the leading behavior of the mass gaps. This is because the eigenvalue associated with the imaginary root no longer corresponds to the lowest state, as can be seen from the behavior of the function $\gamma(\omega)$, given by (4.11a), for $\omega = iv + \pi$. Instead, for $|g| > 1$, the leading eigenvalues are associated with the smallest real solutions of the quantization condition (5.1).

6. SPECTRUM OF THE TRANSFER MATRIX

In this section we obtain the spectrum of the transfer matrix by using the results derived in Sections 3 and 5. First, note that the fermion anticommutation relations satisfied by the spinors Γ_j are invariant under an orthogonal transformation. Hence, the set of $\hat{\Gamma}_j$ defined by

$$\hat{\Gamma} = S^T \Gamma \tag{6.1}$$

satisfy the same anticommutation relation. Furthermore, the creation and annihilation operators

$$X_j^\dagger = \tfrac{1}{2}(\hat{\Gamma}_{2j-1} + i\hat{\Gamma}_{2j}), \qquad X_j = \tfrac{1}{2}(\hat{\Gamma}_{2j-1} - i\hat{\Gamma}_{2j}) \tag{6.2}$$

also satisfy fermion commutation rules. Substituting (6.2) in (2.13), we get

$$V \begin{pmatrix} X_j^\dagger \\ X_j \end{pmatrix} V^{-1} = \begin{pmatrix} e^{\gamma_j} X_j^\dagger \\ e^{-\gamma_j} X_j \end{pmatrix} \tag{6.3}$$

Thus the Hermitean operator V can be expressed in the diagonal form

$$V = \exp\left[-\frac{1}{2} \sum_{j=1}^{M} \gamma_j (2X_j^\dagger X_j - 1) \right] \tag{6.4}$$

With this result, the eigenvalues of the transfer matrix V can be specified in a more familiar form. To this we turn now.

The eigenvalues of the rotation matrix $R_\pm$ are of the form $\exp(\pm\gamma_j)$, where $\gamma_j \equiv \gamma(\omega_j)$, and ω_j $(j = 0, M-1)$ are the solutions of (4.10a). Therefore, the corresponding eigenvalues of the transfer matrix $V_\pm$ have the general form

$$\Lambda = \prod_{j=0}^{M-1} e^{\pm\gamma(\omega_j)/2} \tag{6.5}$$

where the sign for each wavenumber can be chosen independently. The eigenstates of the transfer matrix V consist of the even-parity states from

V_+, and odd-parity states from V_-. This selects the allowed combination of signs in (6.5). Specifically, the parity of vacua of the Fermi fields which bring V to diagonal form is obtained from the following argument. We first inspect the case $K_1^* = 0$, for which $V \equiv V_2$. We then use a continuity argument to get the parity for all $T < T_c$.

For $g > 0$, V_{2-} is brought to diagonal form by the transformation $\hat{\Gamma}_{j-1} = \Gamma_j$ for $j = 2, 3, \ldots, 2M$, and $\hat{\Gamma}_{2M} = \Gamma_1$. This is easily seen by inspection of (2.5). With $g > 0$, V_{2+} is brought to the diagonal form by $\tilde{\Gamma}_{j-1} = \Gamma_j$ for $j = 2, 3, \ldots, 2M$ (as before), but $\tilde{\Gamma}_{2M} = -\Gamma_1$.

The vacua $|\Phi_\pm\rangle$ are given by

$$|\Phi_\pm\rangle = U(S_\pm)\,|0\rangle \tag{6.6}$$

where

$$U(S_\pm)\,\Gamma_j U^\dagger(S_\pm) = \begin{cases} \hat{\Gamma}_j \\ \tilde{\Gamma}_j \end{cases} \tag{6.7}$$

The parity of the vacua are

$$\begin{aligned} i^{2M}\langle \Phi_\pm |\, \Gamma_1, \ldots, \Gamma_{2M}\, |\Phi_\pm\rangle \\ &= \begin{cases} -\langle 0|\, S^\dagger(U_+)\, \tilde{\Gamma}_{2M}\tilde{\Gamma}_1, \ldots, \tilde{\Gamma}_{2M-1} S(U_+)\,|0\rangle \\ +\langle 0|\, S^\dagger(U_-)\, \hat{\Gamma}_{2M}\hat{\Gamma}_1, \ldots, \hat{\Gamma}_{2M-1} S(U_-)\,|0\rangle \end{cases} \\ &= \pm i^{2M}\langle 0|\, \Gamma_1, \ldots, \Gamma_{2M}\,|0\rangle = \pm 1 \end{aligned} \tag{6.8}$$

For $g < 0$, the vacuum parities are just reversed. Finally, with $g = 0$, the (single) vacuum state $|\Phi\rangle$ always has *even* parity.

For $K_1^* \geqslant 0$, we can evaluate $\langle \Phi_\pm |\, \Gamma_1, \ldots, \Gamma_{2M}\, |\Phi_\pm\rangle$ by Wick's theorem in terms of contractions which are continuous functions of K_1^* ($\geqslant 0$). Thus, the $K_1^* = 0$ parity classification holds throughout the region $0 \leqslant T \leqslant T_c$.

With these remarks, some general properties of the TM spectrum are already apparent: For $g > 0$, the largest eigenvalues are given by (6.5) with all signs $+$. The rest of the spectrum is constructed by exciting additional particles. For $g < 0$, however, the parity operators project out the states with an odd number of particles in both subspaces. Therefore, the largest eigenvalues in this case must contain an excitation of the lowest energy level. For $-1 < g < 0$, the lowest energy level corresponds to bound states associated with the imaginary wavenumber given by the solution of (5.2). For $g < -1$, the energy levels corresponding to the imaginary wavenumber are lifted; the lowest excitations in this regime correspond to real wavenumbers $\omega_1^\pm$.

In order to summarize our results for the eigenvalues of the transfer matrix, denote by $\omega_j^{\pm}$ $(j=1,\ldots, M-1)$ the real solutions of (5.1) for $g \gtrless 0$. Here $\omega_1^{\pm}$ are the smallest wavenumbers in each parity subspace; this is obtained with $\beta = -1$. It is convenient to denote

$$\Lambda_{\pm} = e^{\gamma(iv_{\pm})/2} \prod_{j=1}^{M-1} e^{\gamma(\omega_j^{\mp})/2} \tag{6.9}$$

With these conventions, our results for the largest eigenvalues in the odd- and even-parity subspaces can be written in the compact form

	$\frac{1}{2}(1+P_M)\,V_+$	$\frac{1}{2}(1-P_M)\,V_-$
$g>0$	Λ_+	Λ_-
$-1<g<0$	$e^{-\gamma(iv_-)}\Lambda_-$	$e^{-\gamma(iv_+)}\Lambda_+$
$g<-1$	$e^{-\gamma(\omega_1^+)}\Lambda_-$	$e^{-\gamma(\omega_1^-)}\Lambda_+$

(6.10)

For $g>0$ the largest eigenvalue belongs to the odd-parity subspace. This assignment is reversed for $g<0$. The rest of the TM spectrum is easily generated by the creation of additional particles (or pairs of particles) with the wavenumbers given by the quantization condition (4.10a).

Once the TM spectrum is known, the mass gap is easily obtained from the ratio of the two largest eigenvalues. This is considered in the next section.

7. RESULTS FOR THE FINITE LATTICE MASS GAPS

In this section we derive exact results for the behavior of the mass gap for different values of g. The mass gap is obtained from the two leading eigenvalues Λ_0 and Λ_1 of the transfer matrix,

$$m = -\ln(\Lambda_1/\Lambda_0) \tag{7.1}$$

The largest eigenvalues in the even- and odd-parity subspaces, summarized by (6.10), give the leading eigenvalues of V. Before we describe the results for the mass gap for general values of g, let us first examine the special cases $g=+1, 0, -1$, corresponding to periodic, free, and antiperiodic boundary conditions, respectively.

2.1. The Special Cases $g=+1, 0, -1$

Consider first, for simplicity, the case $g=1$, i.e., periodic boundary conditions. In this case all wavenumbers are real and satisfy

$$e^{iM\omega} = \pm 1 \qquad \text{for} \quad V_{\mp} \tag{7.2}$$

This follows from the quantization condition (4.10a), with $Y(1)=0$. Thus, Λ_0 and Λ_1 are the largest eigenvalues of the odd and even subspaces, respectively, and the mass gap can be expressed in the usual integral form

$$m(M)=\frac{1}{2}\left(\sum_{\exp(iM\omega_j)=-1}\gamma(\omega_j)-\sum_{\exp(iM\omega_j)=1}\gamma(\omega_j)\right)$$
$$=-\frac{M}{2\pi}\int_C d\omega\,\gamma(\omega)\left(\frac{1}{e^{iM\omega}+1}+\frac{1}{e^{iM\omega}-1}\right) \quad \text{as} \quad M\to\infty \tag{7.3}$$

where the contour of integration encircles the real axis from $-\pi$ to π, as shown in Fig. 5. By symmetry, the lower and the upper parts of the contour give the same contributions; by periodicity, the upper contour can be deformed to go around the branch cut. As $M\to\infty$, the integral (7.3) is dominated by the neighborhood of the square-root branch point $\omega=i\tau$, where $\tau\equiv 2K_1+\ln(\tanh K_2)$ is the surface tension of an interface orthogonal to the cylinder axis. This reproduces the power law $M^{-1/2}$ as well as the exponential $\exp(-\tau M)$ term in the mass gap for periodic boundary conditions.

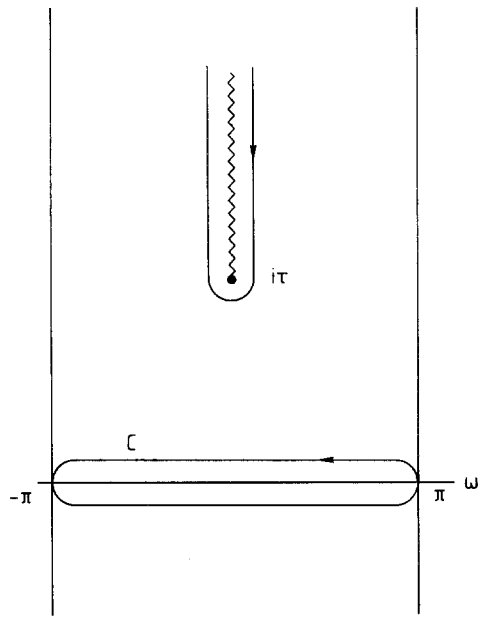

Fig. 5. The contour of integration for (7.3) which can be deformed into the one arround the branch cut.

For the antiperiodic case ($g=-1$), the spectra for the odd and even subspaces are the same as in the periodic case, but the parity assignment is reversed. The maximum eigenvalues are

$$\Lambda_0 = e^{-\gamma(0)}\Lambda_-, \qquad \Lambda_1 = e^{-\gamma(\pi/M)}\Lambda_+ \tag{7.4}$$

where Λ_- and Λ_+ correspond to Λ_0 and Λ_1 of the periodic case, respectively. Since Λ_0 and Λ_1 are exponentially degenerate for $T<T_c$, the mass gap is dominated by the term $\gamma(\pi/M)-\gamma(0)$, which, for large values of M, has the form

$$m(M) = \frac{1}{M^2}\frac{\pi^2}{2\kappa} \tag{7.5}$$

i.e., $\alpha=2$ and $\sigma=0$, where $\kappa=1/\gamma''(0)$ is the *surface stiffness* coefficient. Note that (6.5) confirms the conjecture of refs. 9 and 13, derived on the basis of capillary-wave arguments. In fact, since the quantization condition (6.2) is solved by $\omega_j = j\pi/M$, it follows that *all* finite-size correlation lengths $\xi_j(M)$ in the antiperiodic case agree with those predicted by the capillary-wave theory.[9,13]

In the case of free boundary conditions ($g=0$), the parity is irrelevant. The maximum eigenvalue $\Lambda = \exp[\sum \gamma(\omega)/2]$, with ω satisfying $\exp(iM\omega) = \exp i\delta^*(\omega)$. The lowest energy level γ_0 is associated with the immaginary root, which differs from the branch point $i\tau$ only exponentially. In fact, $\gamma_0 \sim \exp(-M\tau)$. This result was obtained earlier in ref. 17. Hence $\alpha=0$ and $\sigma=\tau$ in this case.

2.2. The Case $g>0$

In the general case $g>0$ the mass gap can be expressed in the form

$$\begin{aligned} m &= -\ln\frac{\Lambda_+}{\Lambda_-} \\ &= \frac{1}{2}\sum_{\beta=\pm 1}\frac{1}{2\pi i}\int_C d\omega\,\gamma(\omega) \\ &\quad \times\left[\frac{iMe^{iM\omega} - i\beta P'(\omega,\beta g)\,e^{iP(\omega,\beta g)}}{e^{iM\omega}-\beta e^{iP(\omega,\beta g)}} - (g\to -g)\right] \end{aligned} \tag{7.6}$$

where $P' \equiv dP/d\omega$. Since g only appears in the product βg, and β is summed over, we change the sign of β in the second term and combine the two terms. This gives

$$m = \sum_{\beta=\pm 1}\frac{\beta}{2\pi}\int_C d\omega\,\gamma(\omega)\frac{e^{iM\omega+iP(\omega,\beta g)}}{e^{2iM\omega}-e^{2iP(\omega,\beta g)}}\,[M-P'(\omega,\beta g)] \tag{7.7}$$

As in the periodic case, we deform the contour so that it goes around the branch cut. When $M \to \infty$, the integral in (7.7) is dominated by $\omega \sim i\tau$ near the branch point; see Fig. 5. The second term in (7.7) scales as $M^{1/2}$ for large M because

$$P'(\omega, \beta g) = Y(\beta g) \cos^2 \frac{P(\omega, \beta g)}{2} \sec^2 \frac{\delta^*(\omega)}{2} \delta'^*(\omega)$$

$$\sim \frac{1}{(\omega - i\tau)^{1/2}} + O[(\omega - i\tau)^{1/2}] \tag{7.8}$$

Hence the first term in (7.7) dominates and gives the same M dependence asymptotically as in the $g = 1$ case, i.e.,

$$m \sim [e^{-iP(i\tau, -g)} - e^{-iP(i\tau, g)}] \frac{e^{-M\tau}}{M^{1/2}} \tag{7.9}$$

with $P(x, y)$ defined by (4.10)–(4.11). This establishes the result $\alpha = 1/2$ and $\sigma = \tau$ for all $g > 0$.

2.3. The Case $-1 < g < 0$

For $-1 < g < 0$, the largest TM eigenvalues can be read off from (6.10). In particular, for the mass gap we get

$$m(M) = \gamma(iv_+) - \gamma(iv_-) - \ln\left(\frac{\Lambda_+}{\Lambda_-}\right) \tag{7.10}$$

For large M, the imaginary solutions v_- and v_+ are exponentially close to each other, as seen from (5.6). The first two terms in (7.10) are of the form $\sim \exp(-Mv_0)$, while the logarithmic term gives the subleading contribution $\sim M^{-1/2} \exp(-M\tau)$. The leading behavior of the mass gap is then

$$m(M) = C \exp(-Mv_0) \tag{7.11}$$

where v_0 can be calculated from (5.3), and C is independent of M; see below. Comparing (7.11) with the general form (1.4), it is clear that $\sigma = v_0$. Using (5.3), we get, after some algebra,

$$\begin{aligned} \sinh \sigma = \mathscr{A} \{ & \cosh 2K_1 \sinh 2K_2 \\ & - \cosh 2K_2 [1 + \mathscr{A}^2 (\sinh^2 2K_1 \sinh^2 2K_2 - 1)]^{1/2} \} \\ & \times (1 - \mathscr{A}^2 \cosh^2 2K_2)^{-1} \end{aligned} \tag{7.12}$$

where

$$\mathscr{A} = (\cosh 2K_2 - \cosh 2gK_2)/(\cosh 2K_2 \cosh 2gK_2 - 1)$$

The graph of σ, obtained from (7.12) for several values of temperature, is shown in Fig. 6. Note that for $g \to 0^-$, $\mathscr{A} \to 1$, and $\sinh \sigma \to \sinh 2(K_1 - K_2^*)$, that is, $\sigma \to \tau$, as expected. In the limit $g \to -1^+$, Eq. (7.12) can be expanded for the small argument, since $\mathscr{A} \to 0$, and we get

$$\sigma \simeq 2K_2(\cosh 2K_1 - \cosh 2K_2^*)(1 - |g|) \tag{7.13}$$

Thus, σ vanishes linearly in the limit $g \to -1^+$ (see also Fig. 6), in agreement with the prediction of Barber and Cates[12] derived by the random walk arguments. Note also that for $g = -1$, the term in the exponent of (7.11) becomes zero. However, the constant C in (7.11), which can be calculated from (7.10), has the form

$$C = \frac{8 \sinh 2K_1 \sinh 2K_2^* \sinh \sigma}{\sinh \gamma(i\sigma)} [Y(|g|)^{-1} - Y(|g|)]^{-1} \left[\frac{d\delta^*}{d\omega}(i\sigma)\right]^{-1} \tag{7.14}$$

and also vanishes. A physically appealing interpretation of the behavior of the mass gap for $-1 < g < 0$ in terms of the tilted interface was given by Zinn-Justin:[11] for $-1 < g < 0$, the perpendicular interface gains energy by tilting at a certain angle, thus creating a segment which runs along the

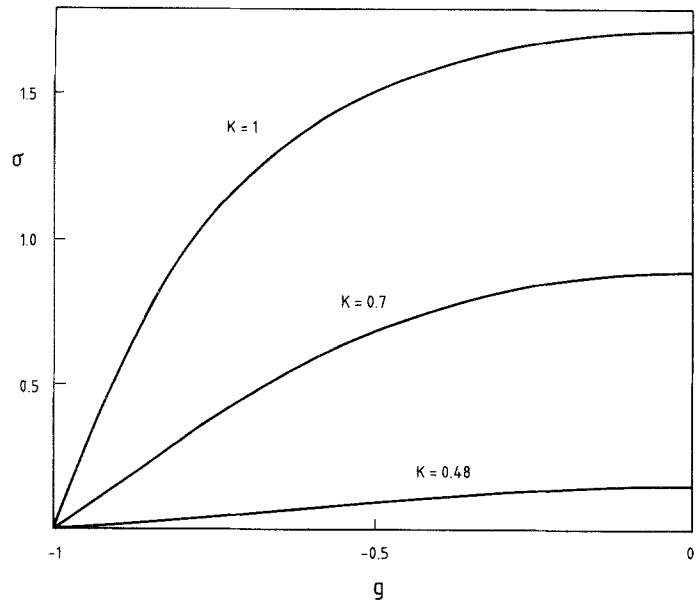

Fig. 6. The graph of σ obtained from (7.12), for different values of temperature (for $K_1 = K_2 = K = J/k_B T$) in the region $-1 < g < 0$.

defect. If τ_d is the free energy associated with the segment of the interface pinned to the defect, then, by minimizing the total energy with respect the tilt angle, it is easy to see that $\sigma \sim (\tau^2 - \tau_d^2)^{1/2}$, where τ is the free energy of the orthogonal interface. (In this minimization the angular dependence of the inclined interface is neglected.) The exact relationship between σ, τ, and τ_d is obtained from (7.12):

$$\cosh \sigma = \cosh \tau - \cosh \tau_d + 1 \tag{7.15}$$

where τ_d is the free energy of an interface pinned to the defect line with couplings $|g| K_2$. The quantity τ_d has been calculated exactly by Abraham.[22] It is obtained as the solution of

$$\cosh \tau_d = \cosh 2K_2 \cosh 2K_1^* - \sinh 2K_2 \sinh 2K_1^* \cosh \varphi \tag{7.16}$$

with φ implicitly given by

$$\cosh 2K_2^*(\cosh 2K_1 e^{\varphi} - \cosh 2K_2^*)$$
$$e^b[\sinh^2 2K_2^* + e^{\varphi}(\cosh \varphi - \cosh 2K_2^* \cosh 2K_1)] = 0 \tag{7.17}$$

and

$$e^b = \frac{\cosh 2K_2}{\cosh 2\,|g|\,K_2} \tag{7.18}$$

Note also that $\tau_d \to \tau$, in the limit $|g| \to 1^-$, so that the relation proposed by Zinn-Justin[11] is recovered in this limit. An exact qualitative derivation of (7.15) is described in the next section.

2.4. The Case $g < -1$

In this case mass gap is given by

$$m(M) = \gamma(\omega_1^-) - \gamma(\omega_1^+) - \ln\left(\frac{\Lambda_+}{\Lambda_-}\right) \tag{7.19}$$

Since Λ_+ and Λ_- are exponentially degenerate, the dominant contribution to the mass gap comes from the first two terms in (7.19). The wavenumbers $\omega_1^{\pm}$ are small, of the order $1/M$, and $\gamma(\omega)$ in (7.19) can be expanded for the small argument

$$\gamma(\omega) = \gamma(0) + \frac{1}{2\kappa}\omega^2 + \cdots \tag{7.20}$$

where κ is the surface stiffness coefficient. Since the wavenumbers $\omega_1^{\pm}$ differ in terms of the order $1/M^2$, then from (7.19) and (7.20), it follows that the mass gap $m(M)$ decays algebraically, with $\alpha = 3$. The exact form is obtained from (7.19) and the appropriate solutions of (5.1), calculated with $\beta = -1$. We get

$$m(M) = \frac{1}{M^3} \frac{\pi^2}{\kappa^2 \sinh 2K_2} [Y(g)^{-1} - Y(g)] \tag{7.21}$$

where we used the small-argument expansion for $\tan \delta^*(\omega)$, (4.11c). This result was predicted by the numerical simulations, and was later derived within the random walk theory.[12] A revealing physical derivation of this result for the quantum case was given by Barber and Cates, who used the second-order perturbation theory.[12]

8. QUALITATIVE ARGUMENTS

The results derived in the previous section can also be recaptured by qualitative arguments. Since such arguments emphasize the physical picture behind the finite-size behavior of the correlation length, it is instructive to describe them in some detail.

Let us first consider the case $g > 0$. In this case the equilibrium state has a succession of closed domain walls which wind around the cylinder. On a cylinder of length N, suppose we have n domain walls. These cannot cross, but are otherwise indistinguishable. Thus, a crude estimate of the n-wall partition function is

$$Z(N, n) \sim Z_0^n(M) \binom{N}{n} \tag{8.1}$$

where $Z_0(M)$ is the partition function of a single domain wall loop; interactions between loops are ignored. A maximization over n yields

$$\frac{N}{n_{\max}} = 1 + \frac{1}{Z_0(M)} \sim 1 + e^{\tau M} \left(\frac{2\pi M}{\kappa} \right)^{1/2} \tag{8.2}$$

by using the results of ref. 24 for $Z_0(M)$. This gives the expected distance between the domain walls, and thus the correlation length and the mass gap of the form (7.9) in the exact work.

When $g < 0$, more care is needed in estimating $Z_0(M)$. As Zinn-Justin[11] has suggested, we expect a section of the closed loop to run along the ladder of negative bonds. The loop is then closed by a free interface at an angle determined by M and the length intercepted with

the ladder. The free energy fluctuations associated with such a crooked configuration are given by

$$f^{\times} \sim M[\sec\theta\tau(\theta) + \tan(\theta)\,\tau_d] \tag{8.3}$$

where τ_d has already been discussed; it is the binding free energy of a domain wall to an internal defect.[22] Note that we *include* angular dependence in τ. We then minimize over θ, using the known result[23] for $\tau(\theta)$:

$$\tau(\theta) = \gamma[\omega_0(\theta)]\cos\theta - i\omega_0(\theta)\sin\theta \tag{8.4}$$

with

$$\gamma^{(\prime)}[\omega_0(\theta)] = i\tan\theta \tag{8.5}$$

The minimization gives $\tau_d = i\omega_0(\theta)$, which allows evaluation of θ from the equation

$$\tan\theta = \frac{\sinh\tau_d \sinh 2K_1^* \sinh 2K_2}{\sinh\gamma(-i\tau_d)} \tag{8.6}$$

This gives

$$Z_0(M) \sim e^{-\sigma M} \tag{8.7}$$

with σ given by (7.15), a result already obtained in the exact analysis. Thus, Zinn-Justin's idea[11] is exactly correct if we put in the *anisotropic* surface tension. Equation (8.7) contains in principle a prefactor. This can be guessed from an SOS model with random displacement parallel to the cylinder axis. A detailed calculation (not reproduced here) gives (8.7) with a prefactor independent of M to leading order. Thus, we recapture the results in (7.11) for $-1 < g < 0$.

The qualitative argument for $g < -1$ takes note that the ground state has a domain wall running along the ladder of bonds and another elsewhere. We develop this by a simple SOS transfer matrix along the cylinder axis for a single strip which avoids the bond ladder, to which the other string remains bound on a microscopic length scale. Using the result of ref. 24 [Eq. (3.10)] for the discrete quantization, we readily recapture the $1/M^3$ mass gap behavior as in (7.21).

ACKNOWLEDGMENTS

We are grateful to V. Privman for numerous useful discussions and critical reading of the manuscript. Research by N.M.Š. has been supported by the National Science Foundation under grant DMR-86-01208. This financial assistance is gratefully acknowledged.

REFERENCES

1. M. E. Fisher, in *Critical Phenomena*, M. S. Green, ed. (Academic Press, New York, 1971).
2. M. N. Barber, in *Phase Transitions and Critical Phenomena*, Vol. 8, C. Domb and J. L. Lebowitz, eds. (Academic Press, New York, 1983).
3. M. E. Fisher and M. N. Barber, *Phys. Rev. Lett.* **28**:1516 (1972).
4. K. K. Mon and D. Jasnow, *Phys. Rev. A* **30**:670 (1984).
5. D. B. Abraham and N. M. Švrakić, *Phys. Rev. Lett.* **56**:1172 (1986).
6. M. P. Nightingale, *J. Appl. Phys.* **53**:7927 (1982).
7. M. E. Fisher and V. Privman, *Phys. Rev. B* **32**:447 (1985).
8. V. Privman and M. E. Fisher, *J. Stat. Phys.* **33**:385 (1983).
9. V. Privman and N. M. Švrakić, *Phys. Rev. Lett.* **62**:633 (1989).
10. G. G. Cabrera and R. Jullien, *Phys. Rev. Lett.* **57**:393 (1986).
11. J. Zinn-Justin, *Phys. Rev. Lett.* **57**:3296 (1986).
12. M. N. Barber and M. E. Cates, *Phys. Rev. B* **36**:2024 (1987).
13. V. Privman and N. M. Švrakić, *J. Stat. Phys.* (1989).
14. T. W. Burkhardt and I. Guim, *Phys. Rev. B* **35**:1799 (1987).
15. P. Pfeuty, *Ann. Phys.* (N.Y.) **57**:79 (1970).
16. M. Henkel, A. Patkos, and M. Schlottmann, Preprint.
17. D. B. Abraham, *Stud. Appl. Math.* **50**:71 (1971).
18. D. B. Abraham and A. Martin-Löf, *Commun. Math. Phys.* **32**:245 (1973).
19. L. Onsager, *Phys. Rev.* **65**:117 (1944).
20. B. Kaufman, *Phys. Rev.* **76**:1232 (1949).
21. D. B. Abraham, L. F. Ko, and N. M. Švrakić, *Phys. Rev. Lett.* **61**:2393 (1988).
22. D. B. Abraham, *J. Phys. A* **14**:L369 (1981).
23. D. B. Abraham and P. Reed, *J. Phys. A* **10**:L121 (1977).
24. N. M. Švrakić, V. Privman, and D. B. Abraham, *J. Stat. Phys.* **53**:1041 (1988).